Surface & Coatings Technology 426 (2021) 127767

Contents lists available at ScienceDirect

Surface & Coatings Technology

journal homepage: www.elsevier.com/locate/surfcoat

Influence of Ag additions on the structure, mechanical properties and oxidation behaviour of CrAlNAg coatings deposited by sputtering

S.S. Rajput [a], S. Gangopadhyay [a,*], A. Cavaleiro [b], A. AL-Rjoub [b], Ch. Sateesh Kumar [c], F. Fernandes [b,*]

[a] Department of Mechanical Engineering, Indian Institute of Technology Bhilai, Raipur 492015, Chhattisgarh, India
[b] University of Coimbra, CEMMPRE - Centre for Mechanical Engineering Materials and Processes, Department of Mechanical Engineering, Rua Luís Reis Santos, 3030-788 Coimbra, Portugal
[c] Madanapalle Institute of Technology and Science, Department of Mechanical Engineering, Angallu 517325, Andhra Pradesh, India

ARTICLE INFO

Keywords:
CrAlNAg coatings
Structure
Chemical bonding
Oxidation
Mechanical properties

ABSTRACT

In this work, the influence of Ag additions into CrAlN coatings on the surface morphology, chemical composition, structure, hardness and oxidation behaviour was studied. Increasing the Ag content decreased the size of the morphological features and produced a more compact coatings. All coatings displayed a fcc structure typical of transition metal nitrides; the silver phase was indexed for the coatings with Ag concentration ≥8.6 at.%. XPS results confirmed that Ag existed as nanoclusters within the coating structure. A maximum hardness of around 23 GPa was observed for the 8.6 at.% of Ag. The decrease of the hardness with further increase in the Ag content was ascribed to the much softer character of this phase. The reference CrAlN coating displayed the best oxidation resistance and the lowest onset point of oxidation. The good oxidation resistance of this coating was attributed to the formation of a continuous and protective thin Cr_2O_3 layer on the top of the oxide layer. Ag additions degraded the oxidation resistance of the coatings, since the diffusion of Ag to the top surface of the oxide scale created extra paths for ions diffusion in the protective Cr-O layer. The formation of $AgCrO_2$ phase in CrAlNAg9 coating, for the particular temperature of at 800 °C, was responsible for the low oxidation resistance of the coating as compared to the same coating oxidized at 900 °C.

1. Introduction

In order to meet the global challenges faced by the machining industries in terms of higher productivity, superior quality, economic competitiveness and development of eco-friendly products and technology, there has been a considerable research interest in the development of high-performance cutting tools which are operating at very high cutting speed to augment the productivity. Therefore, it is imperative that the tool possesses high hardness and wear resistance to withstand the elevated temperature arising during machining. One of the commonly used techniques to mitigate the challenges of tool wear during machining is the use of liquid coolants which can reduce the heat generated during the machining operation and at the same time decrease friction. However, most of the liquid coolants do not sustain their properties and volatilize whilst operating in elevated temperatures, becoming a matter of concern when its vapor condenses or reacts with unrelated parts of the equipment. Another major drawback is the unfavourable impact of liquid coolants on the environment [1].

To circumvent the challenges associated with liquid lubrication, a new family of coatings in the form of adaptive or chameleon types was developed with the aim to automatically and reversibly adjust their surface compositions for the reduction of wear and friction over a wide range of working temperatures [2]. Therefore, these coatings have a great potential to be used in environment-friendly dry machining over that temperature range. The considerable research interest for nanocomposite thin coating and their potential applications in different domains are primarily related to their superior mechanical and tribological properties [3]. Such nanocomposite coatings typically consist of a hard matrix that is highly oxidation resistant, such as CrN, CrAlN, TiAlN, combined with specific elements (metals) which, diffusing up to the surface, form a low friction tribo-layer (e.g., metals as Au, Cu, Ag) [4–8].

Although, soft noble metals like silver and gold are expensive, their amount in these thin coatings is small enough to justify the cost-effectiveness for use as solid lubricants. In particular, researchers

* Corresponding authors.
E-mail addresses: soumya@iitbhilai.ac.in (S. Gangopadhyay), filipe.fernandes@dem.uc.pt (F. Fernandes).

https://doi.org/10.1016/j.surfcoat.2021.127767
Received 17 July 2021; Received in revised form 17 September 2021; Accepted 27 September 2021
Available online 1 October 2021

found that silver has important tribological properties to meet the requirement of a solid lubricant. Silver is very ductile at high temperature, allowing their plastic deformation and consequently allowing easy shear between sliding surfaces and, thus, providing lubrication. Silver also possesses thermochemical stability, such as oxidation resistance at high temperature, which enables to sustain the lubricating performance over a large range of temperatures [9].

Transitional metal nitrides are known for their good balance of toughness and hardness; however, the frictional characteristics are not very promising on dry machining operations. Several researchers have attempted the incorporation of Ag in TiN [10], CrN [11], NbN [12], VN [13], Mo_2N [14], to improve the tribological properties of these coatings but results were not very promising.

According to the general observations, under high temperature operations, Ag diffuses to the top surface of the coating forming clusters all over the surface. The size of the clusters depends on the annealing temperature [15,16]. Moreover, the amount of Ag transport to the surface is dependent on the coating matrix [17,18]. Several studies [11,18–20] have shown that the addition of dispersed Ag nano-particles can improve the tribo-mechanical performance of CrN coating, resulting in lower friction and better wear properties. The presence of Ag debris at the tribological contact has been reported to be responsible for the high temperature lubrication. However, the strong diffusion rate of Ag to the surface often leads to the premature depletion of this element from the bulk of the coating, compromising the lubrication properties and, consequently, limiting their lifetime [8,17,21,22]. Protective thin layers have been applied on the top of the coating [21] resulting in a multilayer architecture [22,23] to control the release of the lubricating phase during the tribological operations. Although some delay on the Ag diffusion was achieved, such strategy did not show effectiveness due to the consumption of the anti-diffusion top layer. An important point to be remarked is the dependence of the properties and performance of Ag rich coatings on the Ag concentration. Higher content of Ag resulted in lower hardness, adhesion and oxidation resistance [23,24].

Chromium nitride (CrN) coating is widely accepted as hard, protective, wear-resistant coatings for cutting tools. Among other single transition metal nitrides, CrN does have a significantly higher oxidation temperature, which is desirable for mechanical applications. To further improve the oxidation resistance of CrN coatings, alloying the system with other metallic elements such as Al has been successfully attempted [25]. Chim et al. reported that CrN coating with Al additions has better hardness and oxidation resistance than CrN, TiN and TiAlN coatings [26]. Mehran et al. concluded that the incorporation of Al into the CrN structure allowed producing denser coatings which enhanced the mechanical and tribological properties [27]. Alloying CrAlN with Ag significantly improved the tribological properties compared to both CrN and CrAlN coatings [7]. Although the CrAlNAg coating displayed ample tribological potential, their oxidation behaviour is yet to be explored in detail. In general, the mechanism of oxidation of ceramic coatings due to addition of Ag is relatively less investigated. Therefore, the present research work aims to investigate the influence of Ag additions on the structure, morphology, mechanical properties and essentially, the oxidation resistance of CrAlNAg coatings deposited by sputtering. Particular emphasis was provided on in-depth characterization of oxide layers at different temperatures.

2. Experimental procedure

2.1. Coatings deposition

The CrAlNAg coatings without and with Ag incorporation were deposited in a semi-industrial PVD coating system manufactured by Teer Coatings Ltd., UK, localized at Instituto Pedro Nunes (IPN), a non-profit private organization for innovation and technology transfer headquartered in Coimbra, Portugal. The schematic representation of the coating chamber is shown in Fig. 1. The chamber has four cathodes evenly distributed in relation to the centre of the chamber. Four targets with 99.99% of purity were used in the depositions: two Cr targets placed in cathode 1 and 3 facing each other and one Al target facing one Ag target. The purity of all the used targets was approximately 99.99%. During the deposition, the substrate table was rotating in the direction from the cathode 1 to cathode 2. Silicon wafers (100) were used as

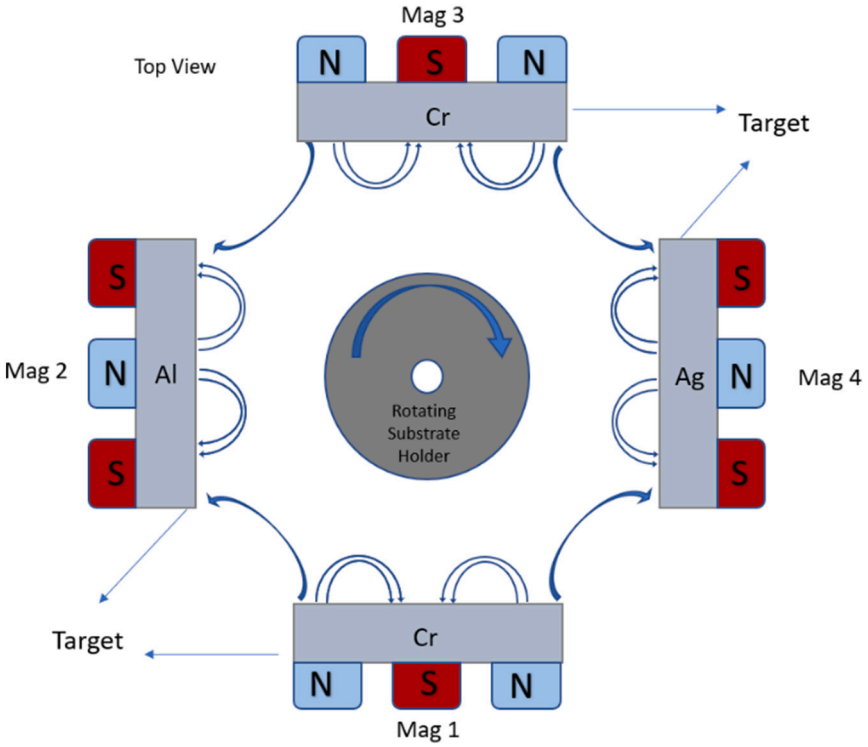

Fig. 1. Schematic representation of the sputtering chamber used for the CrAlNAg coating deposition.

substrate for studying the coatings microstructure, chemical composition, structure and mechanical properties (hardness and Young's modulus), whilst, alumina substrates (10 × 10 × 1 mm) were used for carrying out the oxidation tests.

All the substrates were ultrasonically cleaned with acetone and ethanol for 15 min each before loading them onto the rotating substrate table facing the targets. The substrate table was rotating at 10.5 rpm during deposition. The size of each of the targets was 380 mm × 175 mm × 10 mm and the distance between the targets and the substrate was 150 mm. Prior to the depositions, the chamber was pumped down to a pressure of 4×10^{-4} Pa using a diffusion pump assisted with a rotatory pump. Then, the substrates were etched by Ar ions for 40 min, applying −600 V, frequency of 250 kHz and reverse time of 1.6 μs with a DC-pulsed power supply (Pinnacle Plus, Advanced Energy) connected to the substrate table. Simultaneously, the two Cr targets were cleaned by applying a power 1000 W in each of them, whilst having the shutters in front (for 20 min) and, then, the Al and Ag targets were cleaned for 20 min by moving the shutter to their front and applying a power of 1000 W and 200 W to each of them. The Ar flow during cleaning was 35 sccm, which gave a pressure of 0.25 Pa. Before final depositions, series of interlayer/gradient layers were produced to improve the adhesion of the coating to the substrates as follows: i) a Cr interlayer from the Cr target placed in cathode 3 using a power of 200 W for 10 min, with 35 sccm of Ar (deposition pressure of 0.26 Pa) and applying a pulsed negative voltage bias of 80 V, frequency of 250 kHz and reverse time of 0.5 μs to the substrate, ii) a gradient layer for 10 min, by progressively decreasing the power applied to the Cr target, initially set at 2000 W, down to 1750 W and increasing, simultaneously, the powers applied to the other Cr target from 0 up to 1750 W and to the Al target from 0 up to 3900 W. At the same time, the N flow was increased progressively from 0 up to 31 sccm whereas the Ar flow was kept at 22 sccm. The total thickness of the interlayer + gradient layer was 600 nm. The final coatings were deposited by applying 1750 W to each of the individual Cr targets and 3900 W at the Al target, using the same pulsed bias as applied for the inter-gradient layers. The silver content in the coating was changed by increasing the power applied to the Ag target (0, 100, 200, 260 and 320 W). The Ar and N_2 flows used for the depositions were set to 22 and 31 sccm, respectively. Purity of the Ar and N_2 gases was around 99.9%. The deposition pressure and deposition time were set at 0.41 Pa and 120 min respectively for all the coatings. Deposition rate was calculated by dividing the thickness of the coating by deposition time. Hereinafter, the coating without Ag addition will be designated as CrAlN coating and the coatings with Ag additions will be referenced CrAlNAg-x coatings where x represents the at.% of Ag. The coatings designation and a summary of the deposition conditions are listed in Table 1.

Table 1
Coating denomination, thickness, elemental chemical composition and mechanical properties.

Sample	CrAlN	CrAlNAg2	CrAlNAg9	CrAlNAg12	CrAlNAg16
Coating thickness (μm)	2.6	2.6	3.0	3.1	3.3
Deposition rate (nm/min)	19.8	19.0	23.0	23.7	25.6
Plasma etching	Substrate bias −600 V and 250 kHz (Pulsed DC) for 40 min				
Pulsed DC substrate bias (V)	-80 V (250 kHz)				
Ag power input (Watt)	0	100	200	260	320
Cr (at.%)	37.0	36.5	34.1	32.8	31.1
Al (at.%)	10.9	10.4	9.9	9.3	9.2
N (at.%)	50.0	48.8	45.7	44.1	42.1
Ag (at.%)	0.0	2.4	8.6	11.8	15.8
O (at.%)	2.1	1.9	1.7	2.0	1.8
Cr/Al ratio	3.4	3.5	3.4	3.5	3.4
Hardness (GPa)	18.1	17.0	22.9	19.9	14.4
Young's Modulus (GPa)	280.5 ± 32.8	278.7 ± 23.5	269.0 ± 24.2	251.5 ± 21.5	233.4 ± 24.3

2.2. Characterization

The thickness, surface and fractured cross-section morphologies of the as-deposited coatings were characterized by field emission scanning electron microscopy (FESEM, ZEISS Merlin Gemini2). The chemical composition of the coatings was determined by wavelength dispersive spectroscopy (WDS) in the same equipment. The structure of the coatings was evaluated by X-ray diffraction (XRD, PANalytical Xpert) working with Cu-Kα radiation. The XRD was programmed to operate at current and voltage values of 40 mA and 45 kV, respectively. The XRD diffraction patterns were either acquired in conventional or grazing modes. The scanning range was from 20° to 90° using a step size of 0.04° with 0.5 s acquisition per step. In the glancing incident measurements, the incident angle was set to 3°. The XRD diffraction peaks were fitted using a pseudo-Voigt function. The chemical bonding of the coatings was analyzed by X-ray photoelectron spectroscopy XPS. The analysis was carried out with a monochromatic Al Kα X-ray source (1486.7 eV), operating at 15 kV (90 W), in FAT (Fixed Analyzer Transmission) mode, with a pass energy of 40 eV for the region ROI and 80 eV for the survey. Before analysis, the specimens were etched with Ar ions (2 keV) for 40 min to remove surface contaminations. The effect of the electric charge was corrected using as reference the carbon peak (284.6 eV). The deconvolution of spectra was performed using peak fitting with Gaussian–Lorentzian peak shape and Shirley type background subtraction.

The Hardness and Young's modulus of the coatings were assessed using nano indentation with a Berchovich diamond indenter. Ultra-low load of 15 mN was used to ensure that the depth of indentation was less than 10% of the coating thickness in order to minimize the influence of the substrate hardness. Measurements were carried out at 3 different locations and the mean values were considered.

In order to determine the effect of Ag alloying on the onset point of oxidation and on the oxidation resistance of the CrAlNAg coatings, thermogravimetric analysis (TGA) was carried out in a SETARAM Setsys Ev 1750 thermogravimetric equipment. The coatings deposited onto Al_2O_3 substrates were heated with a constant temperature ramp of 20 °C/min starting from room temperature and went up to 1200 °C to assess the onset point of oxidation. During dynamic and isothermal oxidation tests, the mass gain due to the oxidation was continuously acquired by a microbalance within the TGA equipment having an accuracy of 0.01 mg, at each interval of 2 s. The air flux used during the tests was 50 ml/min. and the heating rate for reaching the isothermal temperature was 20 °C/min. Isothermal tests were then conducted at 800 °C and 900 °C for 2 h in an oven to characterize the oxide scale growth. Those temperatures were selected as they are in the range of temperature expected to have in the final application where the coatings will be applied (for example: tools for machining Ti alloys). After isothermal oxidation tests, the surface and cross section morphology of the oxide scale growth was characterized by SEM. Fractured cross section of the coating was prepared by scratching the reverse side of the coated sample by a diamond indenter followed by breaking. Elemental maps distribution and elemental line profiles were acquired in some cases to characterize the distribution of the elements in the oxide scale. Finally, the types of oxides formed were characterized by XRD diffraction.

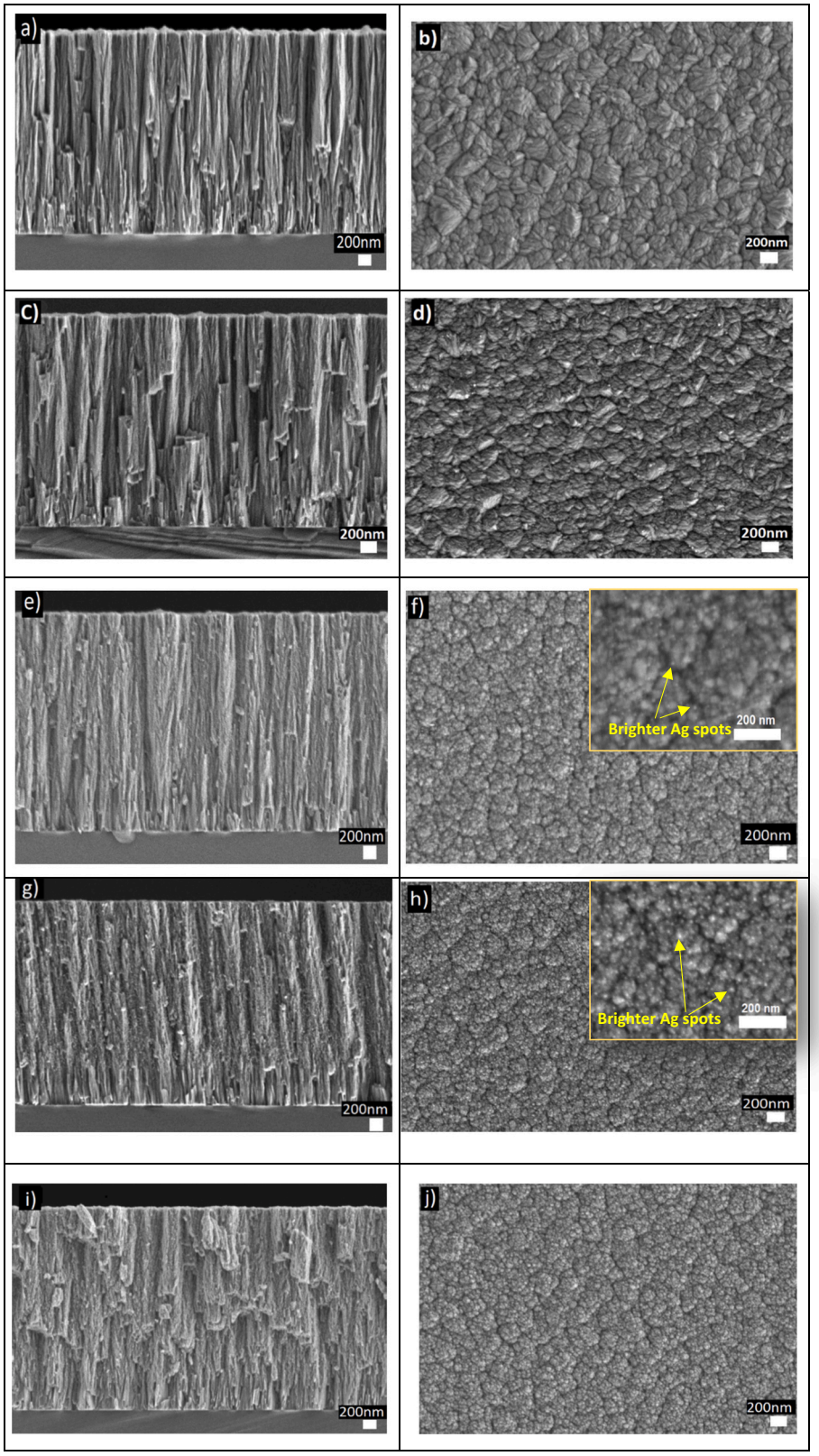

Fig. 2. Cross-section and surface morphology micrographs of the CrAlNAg coatings for: a) and b) CrAlN, c) and d) CrAlNAg2, e) and f) CrAlNAg9, g) and h) CrAlNAg12 and i) and j) CrAlNAg16 (substrate: silicon).

3. Result and discussion

3.1. Chemical composition of coatings

The chemical composition of coatings as measured by WDS is listed in Table 1. As expected, the increase of the power applied to the Ag target allowed to produce coatings with progressive increasing of Ag concentration. All the coatings displayed an approximate stoichiometric composition in relation to (Cr,Al)N when both Cr and Al metallic elements are considered. No significant variations on the Cr/Al ratio with increasing Ag concentration in the coatings were observed, as listed in Table 1.

3.2. Cross-section and surface morphology of the coatings

Fig. 2 shows the cross-section and surface morphologies of CrAlN coatings without and with Ag additions. The reference CrAlN coating displays a columnar morphology. The column tops consisted of aggregates of smaller sized columns, originating features of ~320 nm wide. This type of surface morphology was reported to be caused by the limited surface diffusion due to the relatively low bombardment intensity and low deposition temperature during the coating growth [28]. No changes on the cross-section morphology could be found with the addition of 2.4 at.% Ag to the coating; however, a slight decrease of the size of the surface features could be observed. Further increase of Ag concentration in the coatings up to 15.8 at.% gave rise to a more compact morphology and to a smoother surface. As reported in the literature for other coating systems, Ag addition promotes an increase in the number of nucleation sites, which may be the cause for the increase of the coating's compactness [15,29]. Brighter spots could also be detected on the top surface of the Ag containing coatings, (shown in the inset of Fig. 2f) and h)) which EDS analysis suggested to be Ag nano clusters, in good agreement with other studies [15,30]. From Table 1 and Fig. 2. It is visible that the deposition rate of the coatings slightly decreases for the first Ag concentration and then, progressively increases with the progressive increase of the Ag content. Despite the expected decrease of the deposition rate, due to the excess of N promoted by the extra consumption of Ar at the Ag target, the further increase of the coatings thickness is due to either the additional deposition of Ag or the high sputtering yield of silver as compared to the AlN and CrN compounds [31].

3.3. Structure of the coatings

The XRD diffractograms of the coatings in grazing incidence mode are shown in Fig. 3a). The reference CrAlN coating displayed well crystalline diffraction peaks assigned to a NaCl-type crystalline structure. According to the coating chemical composition, both Cr and Al elements should occupy randomly substitutional positions in the fcc lattice. In fact, according to the literature, the maximum solubility of Al in the CrN structure was reported to be 77 at.% [32] and, above this value, wurtzite phase started to be formed. Accordingly, the wurtzite phase could not be detected in our coatings [33]. It is evident from the XRD pattern of CrAlN coating that all the peaks are shifted to lower diffraction angles in relation to the standard positions of the CrN and AlN ICDD cards. This is indicative of the presence of compressive residual stresses, as reported in several studies [34,35].

The incorporation of Ag in the CrAlN reference coating promoted a progressive increase of the asymmetry of the fcc diffraction peaks, with the appearance of a right shoulder diffraction peak. A deep analysis of these diffraction peaks allows fitting two contributions: one assigned to the fcc CrAlN crystallites and the shoulder peak to the Ag nanoparticles. An image depicting the deconvolution of the (111) and (200) XRD diffraction peaks of CrAlNAg9 and CrAlNAg16 coatings, representative for all the Ag rich coatings, is shown if Fig. 3b). In the case of the CrAlNAg16 coating, a shift of the fcc diffraction peaks to higher angles is

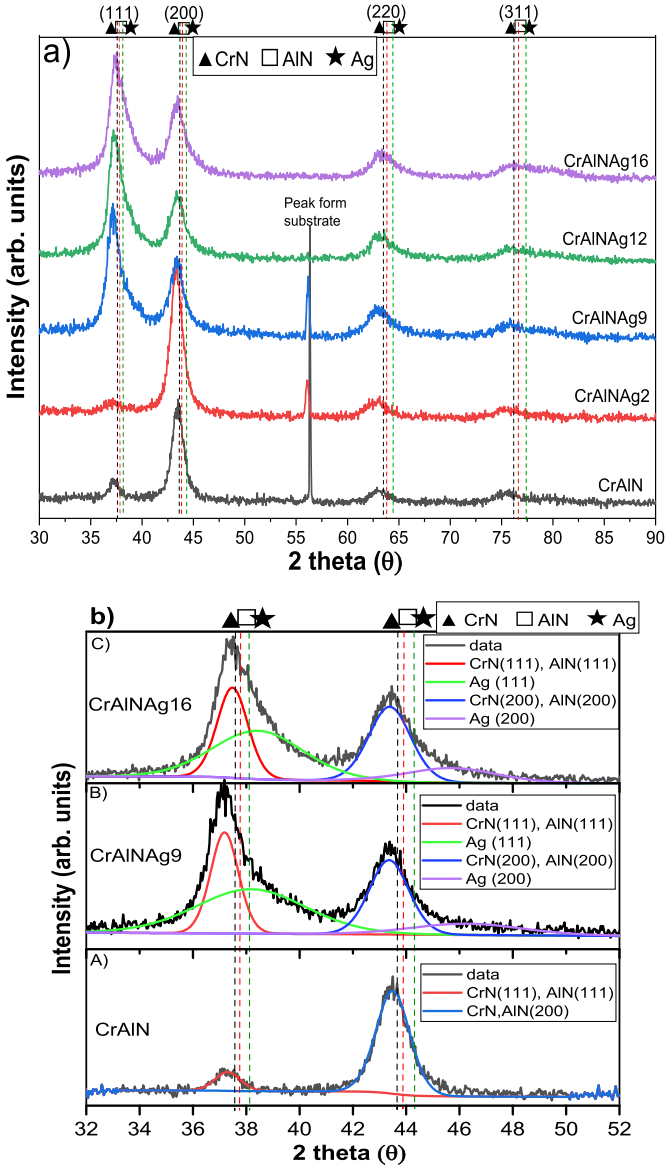

Fig. 3. a) Grazing incident XRD diffraction patterns and b) Deconvolution of the fcc (111) and (200) diffraction peaks of CrAlN, CrAlNAg9 and CrAlNAg16 coatings (substrate: silicon).

observed. This has been reported to be attributed to the incorporation of high amounts of soft Ag on the structure which accommodates the compressive residual stresses and, thus, shifts the fcc XRD diffraction peaks to higher angles [15,36].

3.4. Chemical bonding

The XPS results of Cr, Al, Ag and N of CrAlN, CrAlNAg9 and CrAlNAg12 as-deposited coatings are shown in Fig. 4. Three peak contributions with binding energies of 574.2 eV, 575.1 eV and 577.5 eV can be fitted to the Cr 2p3/2 spectra of all the coatings, corroborating the literature results on CrAlN based coatings [37,38]. The peaks cantered at 574.2 and 575.1 with full width at half maximum (FWHM) of 1.2 eV and 2.5 eV match the typical binding energies of the metallic Cr-Cr and stoichiometric Cr-N [32,33]. On the other hand, the peak at 577.5 eV can be assigned to Cr-O bonds [39], arising from the residual O concentration incorporated in the coating during deposition, in good agreement with the coatings chemical composition, listed in Table 1. Regarding the N 1s core level spectrum, two peak contribution could be

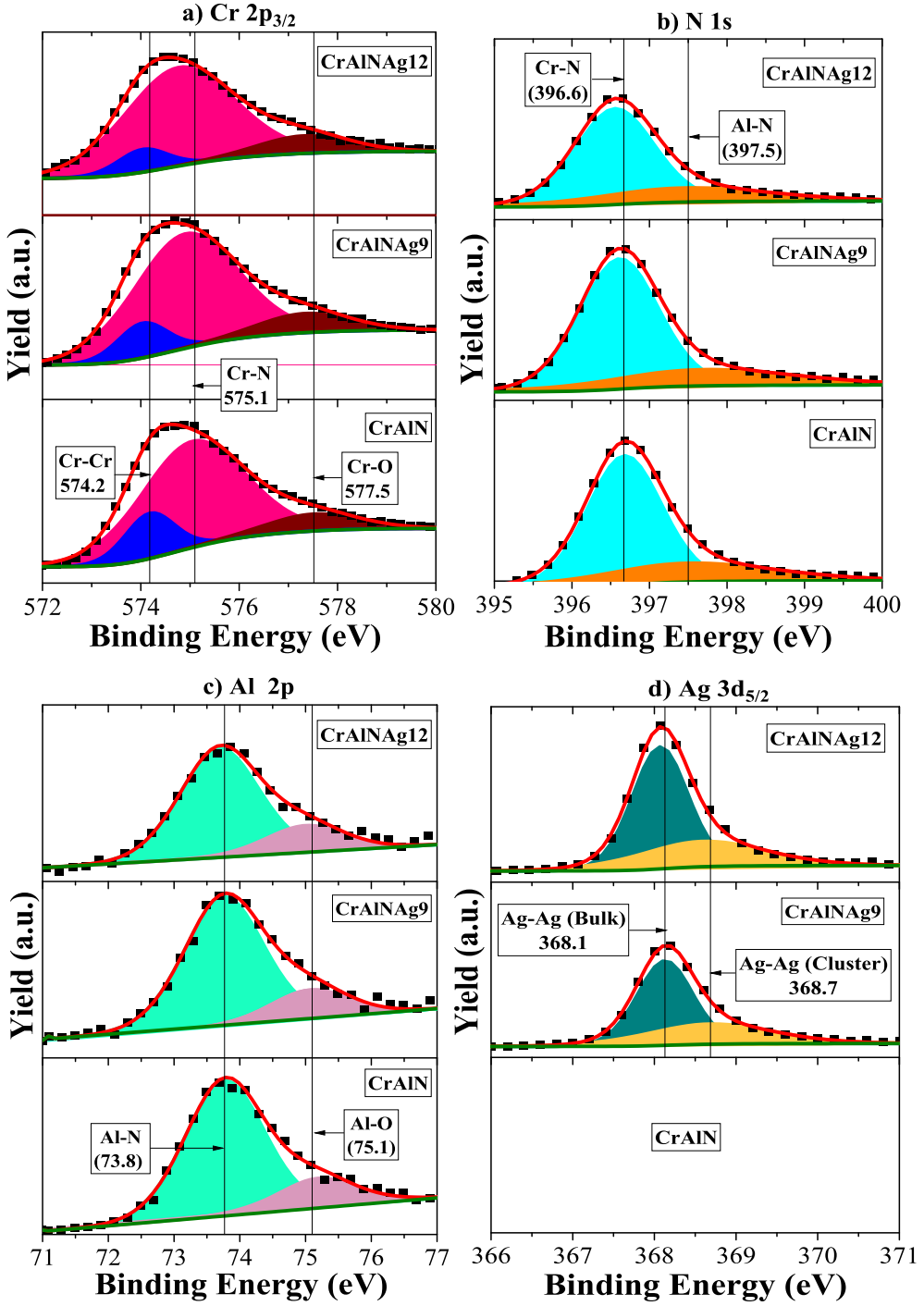

Fig. 4. XPS spectra (a) Cr $2p_{3/2}$, (b) N 1s, (c) Al 2p, and (d) Ag $3d_{5/2}$ for the as-deposited CrAlN, CrAlNAg9 and CrAlNAg12 coatings. The green, scatter, and red lines in the figures are the background correction, the XPS spectra of the samples and the global curve resulting from the fitting, respectively (substrate: aluminium oxide).

fitted: i) the peak at 396.6 eV associated with CrN bonding energy and ii) the peak at 397.5 eV assigned to Al-N bonds [38]. The Al 2p core-level spectrum of all the coatings can also be fitted with two peak contributions with binding energies of 73.8 and 75.1 eV, typical of Al-N and Al-O, respectively [39]. Similarly, to the Cr-O bonding energy fitted to the Cr 2p3/2 spectrum, the presence of the Al-O oxidation state can be justified by the residual O concentration within the coating. Finally, the two components centered at 368.1 and 368.7 eV can be fitted to the Ag $3d_{5/2}$ core level spectrum of Ag rich coatings [40,41]. The former peak is typical of Ag-Ag bulk metallic bonds [42] and the latter Ag-Ag bonds from clusters with sizes smaller than 4 nm, respectively [29]. Similar bands were observed in the literature for other sputtered coating systems (e.g. CrOAg) [29,43,44]. Increasing the Ag concentration in the CrAlN coating did not change the position of any of the previously identified chemical bonds in the different core level spectra, nor the binding energy of the Ag-Ag metallic bonds, suggesting that neighbouring of Cr/Ag atoms did not change. This behaviour may suggest that Ag should be included in the coating as nanoparticles, with very small sizes as suggested by the peak contribution at 367.9 eV in the Ag $3d_{5/2}$ peak, in good agreement with the brighter round features observed on the top surface of the coatings, as shown in Fig. 2.

3.5. Hardness and elastic modulus

The influence of inclusion of Ag in CrAlN on the hardness and Young's modulus of the coating is depicted in Fig. 5. It can be observed that CrAlN exhibited hardness and Young's modulus of 18.1 ± 4.1 GPa and 280.5 ± 32.8 GPa, respectively, which is inside the range of values rereported by some other researchers [45–47]. The decreasing trend of the E values with Ag addition is in accordance with the expectative, since Ag, having a lower Young's modulus than CrAlN, will progressively decrease the value of this property. A similar trend would be expected for the hardness due to the much softer nature of Ag in comparison to CrAlN. The incorporation of a higher amount of soft silver clusters in the microstructure should induce a softening of the coating. However, this decreasing trend is only confirmed in Fig. 5 from 8.6 to 15.8 at. % Ag. From 0 to 2.4 at.% Ag there was hardly any change in hardness. However, a clear improvement of the hardness for the coating with 8.6 at. % Ag (CrAlNAg8) was observed. This increase in hardness may be attributed to the i) slight grain refinement (Hall-Petch effect) caused by the segregation of Ag atoms to the grain boundary of CrAlN grains thus, restricting grain size increase, as observed by Cavaleiro et al. for TiSiN coatings deposited with increasing Ag concentration [15] and, ii) the change in the preferential orientation of the coatings when more than 2 at.% Ag is added to CrAlN coatings. In fact, as in Fig. 3a) a change from (200) to (111) preferential orientation is shown.

3.6. Oxidation process

3.6.1. Continuous oxidation in air

The dynamic thermogravimetric curves of CrAlN, CrAlNAg9, CrAlNAg16 coatings are shown in Fig. 6. The onset temperature for oxidation of CrAlN coating was around 750 °C as obtained by the change in the slope of the curve. This temperature corroborates the work of Trindade et al. [48], where a similar onset point of oxidation was observed for a CrAlN coatings with similar chemical composition. According to the elemental line profiles shown in Fig. S1a) of supplementary material, a very thin oxide layer Cr-O rich has grown on the top of this coating, responsible for the oxidation resistance. The O signal on the remaining zone of the non-oxidized coating should be carefully analyzed since the results may be inaccurate due to overlap between Cr L and O K lines. The addition of 8.6 at. % of Ag to the CrAlN coating only slightly affected the onset point of oxidation (700 °C); nevertheless, a higher oxidation rate was reached revealing the negative influence of silver on the oxidation performance. At ~1030 °C a plateau can be observed, followed by a

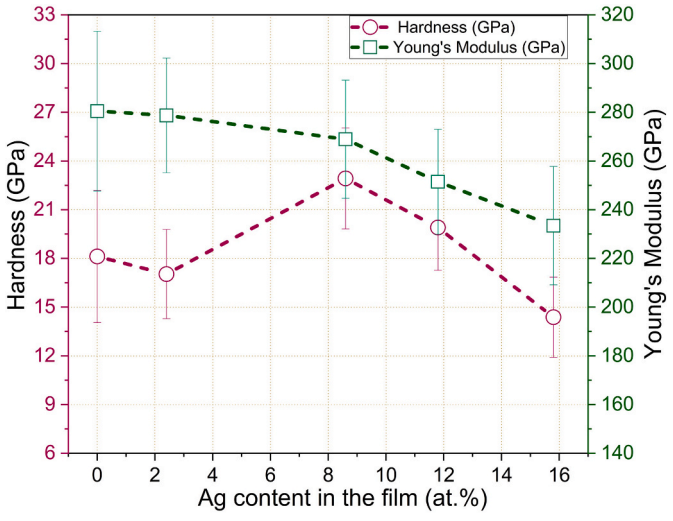

Fig. 5. Hardness and Young's modulus of the CrAlNAg coatings with different Ag contents (substrate: silicon).

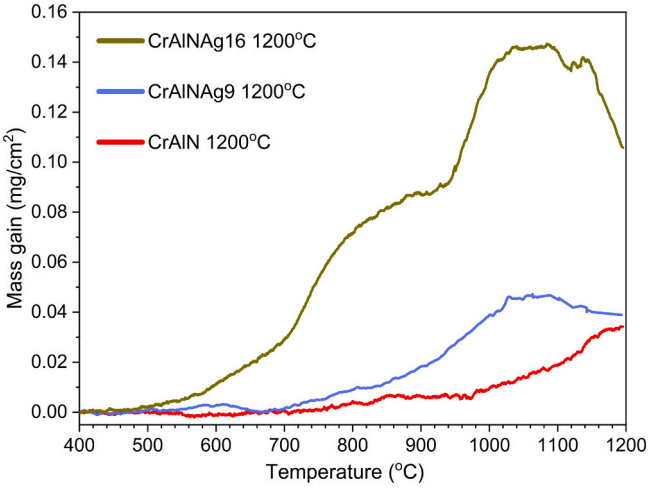

Fig. 6. Thermogravimetric oxidation weight gain of CrAlN, CrAlNAg9 and CrAlNAg16 coatings performed at a constant linear temperature ramp (from RT to 1200 °C at a rate of 20 °C/min) (substrate: aluminium oxide).

drop in the mass gain. Although this horizontal plateau could suggest that the coating was completely oxidized, the cross-section SEM analysis in combination with elemental maps distribution, shown in Fig. S1b) in supplementary material, reveal that an oxide layer was formed on the top, thicker than the one for reference CrAlN coating, but leaving beneath still a thick non-oxidized layer. During the oxidation process, Ag diffused to the surface, creating extra paths for ions diffusion and, consequently, increasing the oxidation rate and the thickness of the oxide scale. The observed decrease of the mass gain is likely due to the evaporation of silver diffused to the surface, as observed by Cavaleiro et al. [24] for TiSi(Ag)N coatings. This conclusion is corroborated by the absence of Ag signals/vestiges on the oxidized layer as shown in the elemental map distribution in Fig. S1b) in supplementary material. Although, the evaporation point of bulk silver is indeed very high 2162 °C, when nanoparticles are considered, it is well known in literature that the size of the particles plays an important role in the decrease of the melting and evaporation temperature of metals i.e. the lower the size of the clusters, lower are the melting and evaporation temperature points [49,50]. This was clearly observed by Asoro.et al. [51] who, by in-situ TEM heating experiments, observed evaporation of silver nanoparticles starting at 580 °C. Thus, taking the literature into account the decrease in mass gain after achieving a saturation in the oxidation mass gain is likely attributed to the evaporation of Ag. With increasing the Ag concentration to 15.8 at.%, the onset of oxidation strongly decreased down to, approximately, 450 °C. Two oxidation processes are observed, one up to ~800 °C and another from this temperature, up to ~1050 °C. Above this temperature, similar to the CrAlNAg9 coating a horizontal plateau was formed followed by a decrease of mass gain. Thus, higher Ag concentrations to CrAlN coating lead to a degradation of the onset point of oxidation and oxidation resistance of the coatings. Cross section morphology of the oxidized specimens and elemental maps distribution in Fig. S1c) in supplementary material reveal the formation of a very thick and complex oxide scale, however, a very small region of the coating which was not oxidized can still be observed near to the interface, showing that despite of this higher oxidation weight gain, the coating was not totally consumed. On the basis of the dynamic oxidation curves, one might conclude that the higher the Ag content in the coatings, lower is the oxidation resistance. In order to understand the growth of oxide scale, isothermal oxidation tests were performed at specific selected isothermal temperatures for 2 h.

3.6.2. Isothermal oxidation

Fig. 7 shows the morphology and corresponding elemental lines

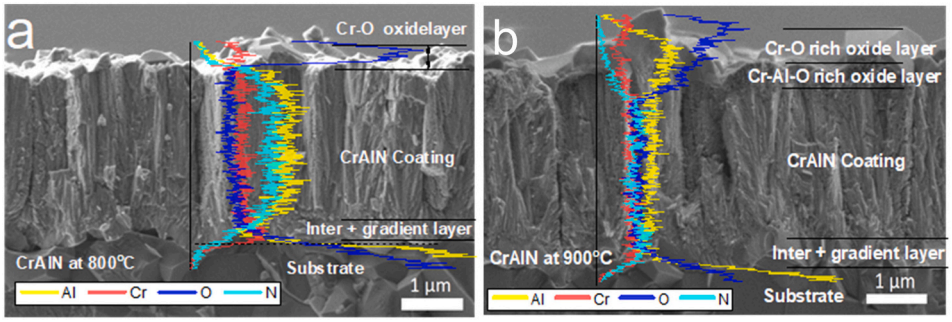

Fig. 7. Cross section morphology and corresponding elemental lines distribution of CrAlN coating oxidized at: a) 800 °C and 900 °C (substrate: aluminium oxide).

distribution on cross section of oxidized reference CrAlN coating at 800 °C and 900 °C for 2 h. The CrAlN coating oxidized at 800 °C resulted in negligible oxide scale as confirmed by the SEM image and the elemental line profiles shown in Fig. 7a); a very thin layer, Cr-O rich, was formed on the top of the coating, whilst no evidence of oxidation of Al could be found as confirmed by the absence of Al signal in the oxide layer. According to the XRD diffraction pattern shown in diffractogram b) in Fig. 8a), this oxide could be indexed as Cr_2O_3 phase. It should be pointed out that Al_2O_3 indexed in the XRD diffraction pattern, was from the alumina substrate. The intense fcc diffraction peaks confirm the low

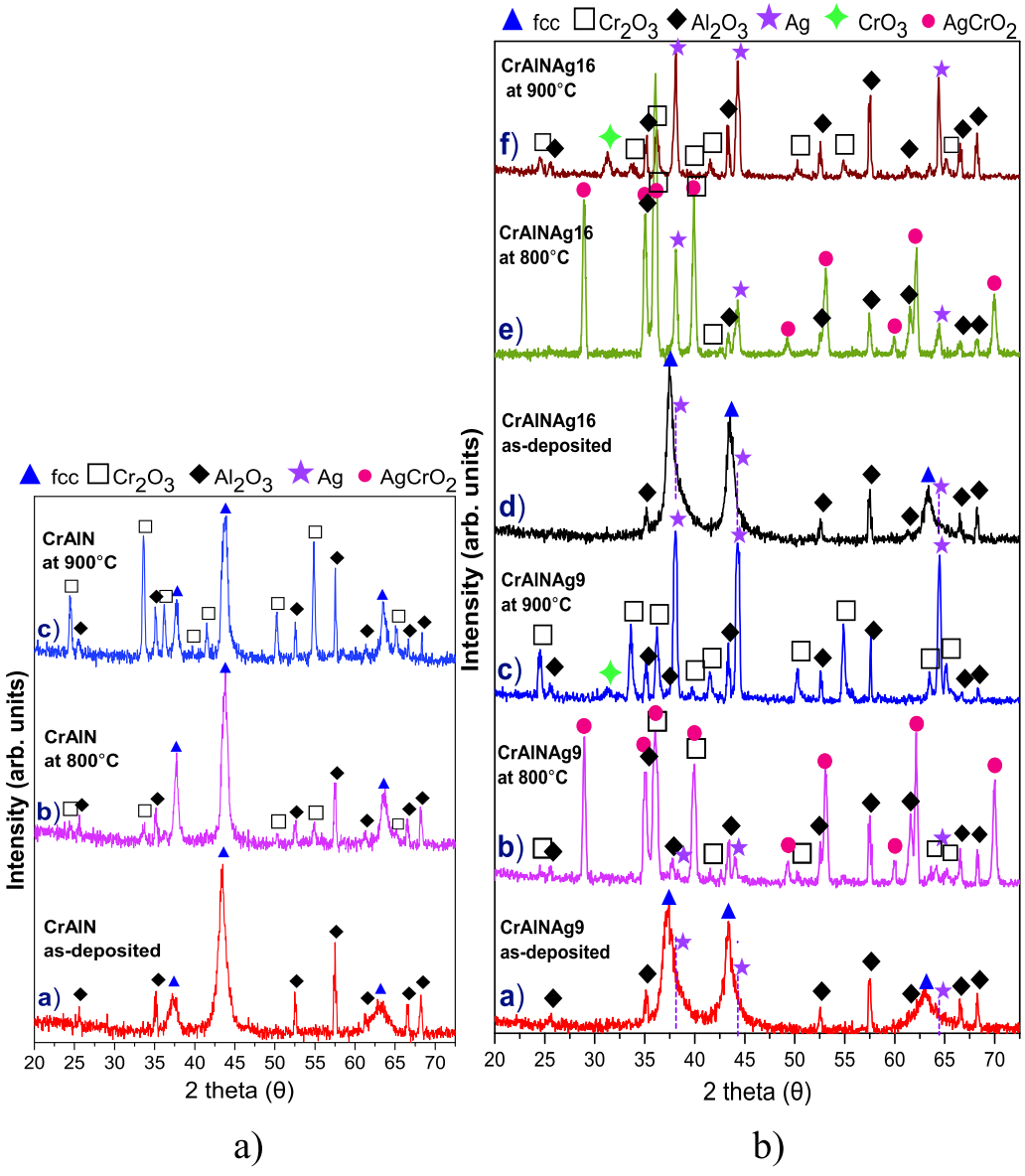

Fig. 8. XRD diffractograms of oxidized coatings. XRD diffraction patterns of as-deposited coatings are plotted, too. Different oxide products were indexed according to the following ICDD cards: (71-1125) - Al_2O_3, (06-0504) – Cr_2O_3, (70-1703) – $AgCrO_2$, (87-0597) – Ag, (32-0285) - CrO_3. (Substrate: aluminium oxide).

oxidation of the coating. However, a shift of the fcc diffraction peaks to higher diffraction angles can be observed, which might be attributed either to the release of residual stresses or to the release of Cr from the fcc structure, as shown by the oxidation process [48]. During oxidation, although Al has more affinity towards O than Cr, due to the lower enthalpy energy formation of Al_2O_3 (−378.2 kcal/mol) as compared to Cr_2O_3 (−252.9 kcal/mol) [52]), Cr-oxide will be preferentially formed due to the much higher Cr concentration in the coating. A continuous protective Cr_2O_3 oxide layer was, thus, established on the top of the coating slowing down the outward diffusion of Cr through the oxide scale and, consequently, protecting the CrAlN coating from oxidation.

When the temperature was raised to 900 °C, the cross-section morphology together with the elemental line profiles shown in Fig. 7b) revealed the formation of a dual oxide layer: a compact Cr-O oxide-rich layer on the top followed by a porous Cr-Al-O oxide layer underneath. These results agree with the previous works, where, during isothermal oxidation tests of coatings with similar chemical composition, a dual oxide layer was grown [53]. Nevertheless, the transition from monolayer to dual-layer structure has been seen to be dependent on the coating's chemical composition and isothermal temperature [54,55]. XRD diffraction pattern of the oxidized coating (see spectrum c) in Fig. 8a)) revealed the formation of Cr_2O_3 and Al_2O_3 oxides. Although Al_2O_3 signal was expected from the substrate, the diffractions peaks from Al_2O_3 increased in intensity when compared to either the as-deposited and the oxidized coating at 800 °C, suggesting the formation of additional Al_2O_3 oxide. The elemental line profiles, together with the oxides detected by XRD, allowed identifying the outer layer as Cr_2O_3 and the inner layer as a mixture of Cr_2O_3 and Al_2O_3 phases. Similarly, during the oxidation test at 800 °C, due to the higher Cr concentration in the coating Cr_2O_3 layer will start to grow on the top surface. However, due to the enhanced diffusion at this temperature Al_2O_3 was also formed. The oxidation proceeded by Cr ions diffusing outward the oxide scale to the interface between oxide and open air and inward diffusion of O [56]. Due to the Cr outward diffusion, a porous Cr-Al-O rich oxide layer was left behind and a protective and continuous Cr_2O_3 oxide layer was grown on top. Over time, the increase of the thickness of the oxide scale would progressively slow down the kinetics ions diffusion.

CrAlNAg9 coating oxidized at 800 °C (shown in Fig. 9a)) displayed a thicker oxide scale than reference CrAlN coating tested at 900 °C, clearly revealing a loss of the oxidation resistance when Ag is added to the coating. On the top, a layer rich in Ag-Cr-O was formed, followed by a Cr-Al-O rich layer with minor traces of Ag. The strong signal of the silver mixed with Cr in the outer layer suggests a different oxidation mechanism in relation to CrAlN. Instead of having the preferential oxidation of Cr from the CrAlNAg material, the mixed $AgCrO_2$ oxide was formed as confirmed by the XRD diffraction pattern (see spectrum b in Fig. 8b)). Cr_2O_3 was also identified which was probably originated from the Al-Cr-O oxide layer which shows a weak signal of Ag. The very shallow diffraction peaks assigned to pure Ag suggests the existence of pure Ag very probably from the non-oxidized coating. The surface morphology of the oxidized coating displayed small plate-like features homogeneously distributed on the surface (See Fig. S2a) in supplementary material). As expected, no signs of Ag particles can be observed.

When the temperature was increased to 900 °C, unexpectedly, a thinner oxide scale, when compared to 800 °C, was observed, suggesting that this coating has a better oxidation resistance for higher temperatures (see Fig. 9). A three-layer oxide scale was formed (Fig. 9b): i) spherical agglomerates of Ag on top (see Fig. S2b) of supplementary material), followed by ii) a very thin Cr-O layer and, underneath, iii) a thick Cr-Al-O layer with minor signals of Ag. Contrarily to the temperature of 800 °C, no $AgCrO_2$ phase could be detected by XRD (see spectrum c in Fig. 9), as confirmed by the cross-section elemental maps distributions since no overlap between Cr, O and Ag signals was observed on the top of the oxide scale (Fig. 9b)). According to the literature, $AgCrO_2$ is very unstable and at temperatures higher than 850 °C, it decomposes into Ag and Cr_2O_3 phases [57,58]. Therefore, the higher oxidation, observed for the CrAlNAg9 coating at 800 °C, as compared to 900 °C, is likely due to the $AgCrO_2$ phase, which impeded the formation of the protective Cr-O layer as it was observed for the CrAlN coating. $AgCrO_2$ layer was found to be discontinuous (see Fig. S2 in supplementary material) without providing an efficient barrier to ions diffusion and, therefore, a protective character. At 900 °C, XRD shows a pattern with most of the diffraction peaks very similar to the ones found for CrAlN with the formed oxides being more protective and responsible for the higher oxidation resistance at this temperature. In addition to these peaks, strong intense diffraction ones assigned to Ag could be detected in good agreement with the formation of the Ag spheres observed on the top of the oxidized scale. Similar to 800 °C, the elemental map's distribution revealed that the majority of Ag diffused out from the inner oxide scale. Cr_2O_3 and Al_2O_3 phases could also be indexed in the XRD diffractograms, suggesting that the external Cr-O layer was Cr_2O_3 and the Cr-Al-O rich layer was a mixture of Cr_2O_3 and Al_2O_3 phases.

Similar oxide scale and phases (see XRD diffraction patterns e) in Fig. 8) as for CrAlNAg9 coating oxidized at 800 °C was also observed for CrAlNAg16 coating oxidized at the same temperature. However, a

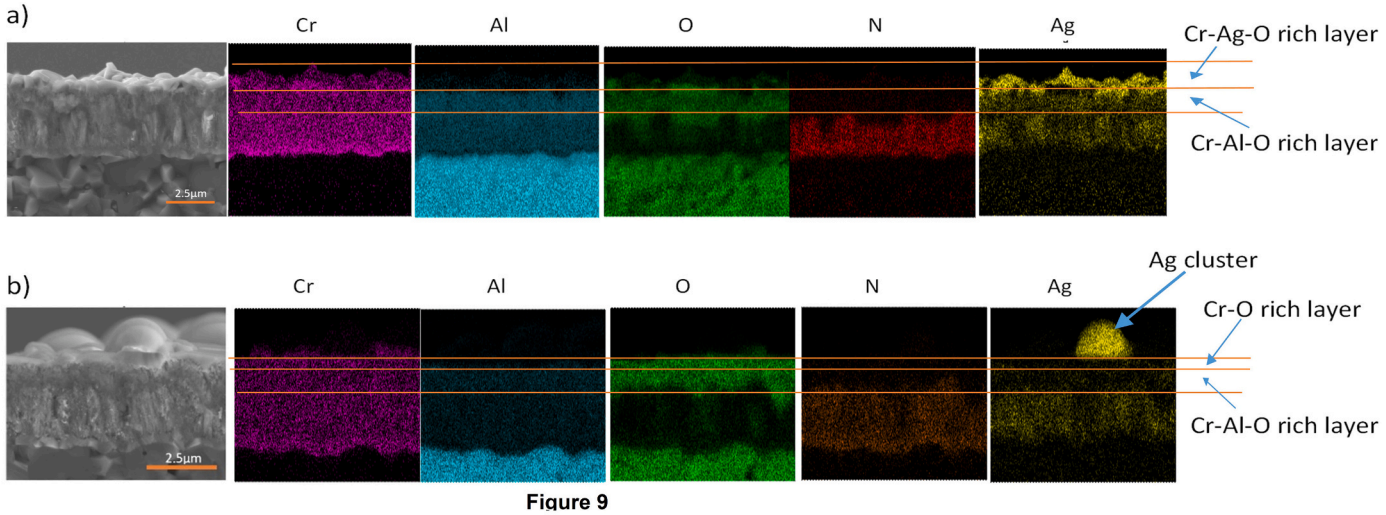

Figure 9

Fig. 9. Cross-section morphology and corresponding elemental maps distribution of CrAlNAg9 coating oxidized at: a) 800 °C and b) 900 °C (substrate: aluminium oxide).

thicker oxide scale was formed, in good agreement with the dynamic oxidation curves which suggested an increase of mass gain due to oxidation with increase in Ag content. For isothermal oxidation test at 900 °C, CrAlNAg16 coating was revealed to be totally oxidized (see Fig. S3 in supplementary material). Similar oxide scale and phases, as identified for CrAlNAg9 coating at 900 °C, could be observed/detected. The formation of bigger Ag spheres on top of the oxide scale (see Fig. S2c) in supplementary material) suggests that in this coating the diffusion of Ag to the surface was higher than for CrAlNAg9 coating. This clearly reveals that higher the Ag concentration on the coatings, higher is the diffusion of silver to the top surface and, consequently, higher paths for ions diffusion are open, thus, decreasing the oxidation resistance. In all the isothermal tests, the possibility of evaporation of Ag should not be ruled out since the Ag was primarily present in the form of nanoparticles and could easily evaporate at current isothermal temperatures as shown by references [24,51],

In conclusion, the oxidation of Ag rich CrAlN coatings proceeded in similar way as pure CrAlN coating, however, the presence of Ag and its diffusion to the surface, modified the Cr-O protective layer creating extra ions diffusion paths and giving rise to a lower oxidation resistance. In the case of CrAlNAg9 coating oxidized at 800 °C, the oxidation resistance was even lower as compared to 900 °C due to the formation of a low ion diffusion protective $AgCrO_2$ phase on top of the oxide scale layer. Although such phase was also formed in CrAlNAg16 coating oxidized at 800 °C, the coating was totally oxidized at 900 °C. This was caused by the higher amount of Ag on the coating which strongly diffused to the surface as suggested by the dynamic oxidation curves shown in Fig. 6 and confirmed by the surface morphology of the coating shown in Fig. S2 in the supplementary material.

An attempt was made to compare the results of oxidation studies of ceramic-Ag coatings reported in the literature. Oxidation during tribotesting of VCN-(Ag) coating was investigated by Bondarev et al. [59]. It was observed that the addition of Ag caused a reduction in oxidation threshold and more intensive oxidation of the coating. Incorporation of Ag reduced the onset point of the oxidation of VCN coating from 400 °C to 325 °C and resulted in higher rate of mass gain during oxidation. Cavaleiro et al. [24] reported that although introduction of Ag in TiSiN coating did not change the onset point of oxidation (~800 °C), it degraded their oxidation resistance. AL-Rjoub et al. [23] observed that the onset point of oxidation of multi-layered TiSiN/TiAgN coatings was 700 °C and did not change with Ag additions. However, a lower oxidation performance was observed with Ag additions. Considering that the starting point of oxidation of the coatings studied in this work is in the range of the values reported in the literature for other ceramics systems, these coatings may be of interest in tribological applications. Further studies will be devoted to their tribological and machining performance.

4. Conclusion

The current research work investigated the influence of Ag addition on the chemical composition, morphology, structure, mechanical properties, and oxidation resistance of CrAlNAg coatings. The Ag content was varied in the range from 0 up to 15.8 at.% with increasing the power applied to the Ag target. SEM surface analysis also confirmed the presence of Ag as small clusters. All the coatings displayed an fcc NaCl-type structure characteristic of several transition metal nitrides. XPS analysis confirmed the formation of Ag-Ag bond in the position of Ag as nanoparticles. A maximum hardness of 23 GPa was observed for the coating with 8.6 at.% of Ag. For the higher content of Ag, a reduction in the hardness occurred owing to the softer character of the Ag phase. TGA analysis showed that the onset point of oxidation of CrAlN coating was reached at ~700 °C. Ag additions up to 8.6 at.% of Ag (CrAlNAg9) did not change the starting point of oxidation. However, further increase in the Ag content (CrAlNAg16) deteriorated the oxidation resistance by either a much earlier initiation of the oxidation or higher rate of mass gain. The observed decrease of the mass gain after achieving a saturation in the oxidation mass gain was attributed to the evaporation of Ag at high temperatures. Isothermal oxidation results revealed the formation of distinct oxide products depending on the coatings' chemical composition and isothermal temperature. The reference CrAlN coating displayed the best oxidation resistance due to the formation of a continuous thin Cr_2O_3 layer on the top of the oxide scale. The additions of 8.6 and 15.8 at. % of Ag (CrAlNAg9 and CrAlNAg16 coatings) showed the formation of an $AgCrO_2$ layer followed by a Cr-Al-O layer when the coating was oxidized at 800 °C. The first was responsible for a low oxidation resistance. For 900 °C, $AgCrO_2$ layer was not formed anymore. However, at this temperature, spherical Ag particles could be observed at the top of the oxide scale suggesting the diffusion of Ag to the top. Such, phenomenon interfered in the formation of the protective Cr-O layer creating extra paths for the ion diffusion and lowering the oxidation resistance in relation to CrAlN. The current study clearly indicates that a good balance of the mechanical properties can be accomplished with the incorporation of 8.6 at.% of Ag in CrAlN coating with only a minor sacrifice in oxidation resistance. This result allows envisaging the potential of these coatings to be used in applications where silver can work as lubricant without losing the necessary mechanical strength.

CRediT authorship contribution statement

S.S. Rajput: Conceptualization, Investigation, Methodology, Validation, Writing – original draft. **S. Gangopadhyay:** Supervision, Conceptualization, Investigation, Validation, Writing – review & editing, Resources, Project administration, Funding acquisition. **A. Cavaleiro:** Project administration, Conceptualization, Writing – review & editing. **A. AL-Rjoub:** Investigation, Writing – review & editing. **Ch. Sateesh Kumar:** Investigation, Writing – review & editing. **F. Fernandes:** Supervision, Conceptualization, Investigation, Validation, Writing – review & editing, Resources, Project administration, Funding acquisition.

Declaration of competing interest

The authors declare that they have no known competing financial interests or personal relationships that could have appeared to influence the work reported in this paper.

Acknowledgments

S. Gangopadhyay would like to thank the Department of Science and Technology, Government of India for funding the research work under the bilateral collaborative project between India and Portugal (Project No. DST/INT/Portugal/P-14/2017). This research is also sponsored by FEDER Funds through Portugal 2020 (PT2020), by the Competitiveness and Internationalization Operational Program (COMPETE 2020) and national founds through the Portuguese Foundation for Science and Technology (FCT), under the projects: SMARTLUB – ref. "POCI-01-0145-FEDER-031807", MCTool21- ref: "POCI-01-0247-FEDER-045940" and CEMMPRE - ref. "UIDB/00285/2020". Bilateral collaborative project between Portugal and India (Project number 441.00 INDIA) is also acknowledged.

Appendix A. Supplementary data

Supplementary data to this article can be found online at https://doi.org/10.1016/j.surfcoat.2021.127767.

References

[1] S. Debnath, M.M. Reddy, Q.S. Yi, Environmental friendly cutting fluids and cooling techniques in machining: a review, J. Clean. Prod. 83 (2014) 33–47, https://doi.org/10.1016/j.jclepro.2014.07.071.

[2] C. Muratore, A.A. Voevodin, Chameleon coatings: adaptive surfaces to reduce friction and wear in extreme environments, Annu. Rev. Mater. Res. 39 (2009) 297–324, https://doi.org/10.1146/annurev-matsci-082908-145259.

[3] C.C. Tseng, J.H. Hsieh, S.C. Jang, Y.Y. Chang, W. Wu, Microstructural analysis and mechanical properties of TaN-Ag nanocomposite thin films, Thin Solid Films 517 (2009) 4970–4974, https://doi.org/10.1016/j.tsf.2009.03.136.

[4] B. Kim, Microstructure and tribological behavior of CrN-Cu nanocoatings deposited by PVD systems, in: SAE Technical Papers, 2016, pp. 1–4, https://doi.org/10.4271/2016-01-0492.

[5] C.P. Mulligan, D. Gall, CrN-Ag self-lubricating hard coatings, Surf. Coat. Technol. 200 (2005) 1495–1500, https://doi.org/10.1016/j.surfcoat.2005.08.063.

[6] H.D. Mejía V., D. Perea, G. G.B., Development and characterization of TiAlN (Ag, cu) nanocomposite coatings deposited by DC magnetron sputtering for tribological applications, Surf. Coat. Technol. 381 (2020), 125095, https://doi.org/10.1016/j.surfcoat.2019.125095.

[7] P. Basnyat, B. Luster, Z. Kertzman, S. Stadler, P. Kohli, S. Aouadi, J. Xu, S. R. Mishra, O.L. Eryilmaz, A. Erdemir, Mechanical and tribological properties of CrAlN-Ag self-lubricating films, Surf. Coat. Technol. 202 (2007) 1011–1016, https://doi.org/10.1016/j.surfcoat.2007.05.088.

[8] C.P. Mulligan, T.A. Blanchet, D. Gall, CrN-Ag nanocomposite coatings: effect of growth temperature on the microstructure, Surf. Coat. Technol. 203 (2008) 584–587, https://doi.org/10.1016/j.surfcoat.2008.06.052.

[9] H.E. Sliney, Role of Silver in Self-lubricating Coatings for Use at Extreme Temperatures, 1985, https://doi.org/10.1080/05698198608981698.

[10] J.G. Han, H.S. Myung, H.M. Lee, L.R. Shaginyan, Microstructure and Mechanical Properties of Ti – Ag – N and Ti – Cr – N Superhard Nanostructured Coatings vol. 175, 2003, pp. 738–743, https://doi.org/10.1016/S0257-8972.

[11] C.P. Mulligan, T.A. Blanchet, D. Gall, CrN-Ag nanocomposite coatings: tribology at room temperature and during a temperature ramp, Surf. Coat. Technol. 204 (2010) 1388–1394, https://doi.org/10.1016/j.surfcoat.2009.09.018.

[12] D.S. Stone, J. Migas, A. Martini, T. Smith, C. Muratore, A.A. Voevodin, S. M. Aouadi, Adaptive NbN/Ag coatings for high temperature tribological applications, Surf. Coat. Technol. 206 (2012) 4316–4321, https://doi.org/10.1016/j.surfcoat.2012.04.054.

[13] S.M. Aouadi, D.P. Singh, D.S. Stone, K. Polychronopoulou, F. Nahif, C. Rebholz, C. Muratore, A.A. Voevodin, Adaptive VN/Ag nanocomposite coatings with lubricious behavior from 25 to 1000 °c, Acta Mater. 58 (2010) 5326–5331, https://doi.org/10.1016/j.actamat.2010.06.006.

[14] W. Gulbi, T. Suszko, Thin films of Mo2N/Ag nanocomposite — the structure, mechanical and tribological properties 201 (2006) 1469–1476, https://doi.org/10.1016/j.surfcoat.2006.02.017.

[15] D. Cavaleiro, S. Carvalho, A. Cavaleiro, F. Fernandes, TiSiN(Ag) films deposited by HiPIMS working in DOMS mode: effect of Ag content on structure, mechanical properties and thermal stability, Appl. Surf. Sci. 478 (2019) 426–434, https://doi.org/10.1016/j.apsusc.2019.01.174.

[16] L. Incerti, A. Rota, S. Valeri, A. Miguel, J.A. García, R.J. Rodríguez, J. Osés, Nanostructured self-lubricating CrN-Ag films deposited by PVD arc discharge and magnetron sputtering, Vacuum. 85 (2011) 1108–1113, https://doi.org/10.1016/j.vacuum.2011.01.022.

[17] P.A. Papi, C.P. Mulligan, D. Gall, CrN-Ag nanocomposite coatings: control of lubricant transport by diffusion barriers, Thin Solid Films 524 (2012) 211–217, https://doi.org/10.1016/j.tsf.2012.10.010.

[18] C.P. Mulligan, T.A. Blanchet, D. Gall, CrN-Ag nanocomposite coatings: high-temperature tribological response, Wear. 269 (2010) 125–131, https://doi.org/10.1016/j.wear.2010.03.015.

[19] P.J. Kelly, H. Li, P.S. Benson, K.A. Whitehead, J. Verran, R.D. Arnell, I. Iordanova, Comparison of the tribological and antimicrobial properties of CrN/Ag, ZrN/Ag, TiN/Ag, and TiN/Cu nanocomposite coatings, Surf. Coat. Technol. 205 (2010) 1606–1610, https://doi.org/10.1016/j.surfcoat.2010.07.029.

[20] M. Baraket, D. Mercs, Z.G. Zhang, C. Coddet, Mechanical and tribological properties of CrN/Ag and CrSiN/Ag nanoscale multilayers, Surf. Coat. Technol. 204 (2010) 2386–2391, https://doi.org/10.1016/j.surfcoat.2010.01.004.

[21] C.P. Mulligan, T.A. Blanchet, D. Gall, Control of lubricant transport by a CrN diffusion barrier layer during high-temperature sliding of a CrN-Ag composite coating, Surf. Coat. Technol. 205 (2010) 1350–1355, https://doi.org/10.1016/j.surfcoat.2010.07.071.

[22] A. Al-rjoub, A. Cavaleiro, S.S. Rajput, F. Fernandes, High Si multilayered TiSiN/TiN (Ag) films with superior oxidation resistance, J. Mater. Res. Technol. 12 (2021) 2340–2347, https://doi.org/10.1016/j.jmrt.2021.04.040.

[23] A. AL-Rjoub, A. Cavaleiro, F. Fernandes, Influence of Ag alloying on the morphology, structure, mechanical properties, thermal stability and oxidation resistance of multilayered TiSiN/Ti(Ag)N films, Mater. Des. 192 (2020), 108703, https://doi.org/10.1016/j.matdes.2020.108703.

[24] D. Cavaleiro, A. Cavaleiro, S. Carvalho, F. Fernandes, Oxidation behaviour of TiSiN (Ag) films deposited by high power impulse magnetron sputtering, Thin Solid Films 688 (2019), https://doi.org/10.1016/j.tsf.2019.137423.

[25] H.C. Barshilia, N. Selvakumar, B. Deepthi, K.S. Rajam, A comparative study of reactive direct current magnetron sputtered CrAlN and CrN coatings, Surf. Coat. Technol. 201 (2006) 2193–2201, https://doi.org/10.1016/j.surfcoat.2006.03.037.

[26] Y.C. Chim, X.Z. Ding, X.T. Zeng, S. Zhang, Oxidation resistance of TiN, CrN, TiAlN and CrAlN coatings deposited by lateral rotating cathode arc, Thin Solid Films 517 (2009) 4845–4849, https://doi.org/10.1016/j.tsf.2009.03.038.

[27] Q.M. Mehran, A.R. Bushroa, M.A. Fazal, Evaluation of CrAlN multilayered coatings deposited by PVD magnetron sputtering, J. Adhes. Sci. Technol. 29 (2015) 2076–2089, https://doi.org/10.1080/01694243.2015.1054577.

[28] M. Athmani, A. AL-Rjoub, D. Cavaleiro, A. Chala, A. Cavaleiro, F. Fernandes, Microstructural, mechanical, thermal stability and oxidation behavior of TiSiN/CrVxN multilayer coatings deposited by D.C. reactive magnetron sputtering, Surf. Coat. Technol. 405 (2021), 126593, https://doi.org/10.1016/j.surfcoat.2020.126593.

[29] F. Fernandes, T.B. Yaqub, A. Cavaleiro, Influence of Ag additions on the structure, mechanical properties and oxidation behaviour of Cr-O coatings deposited by HiPIMS, Surf. Coat. Technol. 339 (2018) 167–180, https://doi.org/10.1016/j.surfcoat.2018.02.025.

[30] H. Köstenbauer, G.A. Fontalvo, C. Mitterer, J. Keckes, Tribological properties of TiN/Ag nanocomposite coatings, Tribol. Lett. 30 (2008) 53–60, https://doi.org/10.1007/s11249-008-9312-7.

[31] N. Laegreid, G.K. Wehner, Sputtering yields of metals for ar+ and ne+ ions with energies from 50 to 600 ev, J. Appl. Phys. 32 (1961) 365–369, https://doi.org/10.1063/1.1736012.

[32] A. Sugishima, H. Kajioka, Y. Makino, Phase transition of pseudobinary Cr-Al-N films deposited by magnetron sputtering method, Surf. Coat. Technol. 97 (1997) 590–594, https://doi.org/10.1016/S0257-8972(97)00402-7.

[33] Y. Makino, K. Nogi, Synthesis of pseudobinary Cr-Al-N films with B1 structure by rf-assisted magnetron sputtering method, Surf. Coat. Technol. 98 (1998) 1008–1012, https://doi.org/10.1016/S0257-8972(97)00391-5.

[34] L.B. Varela, F. Fernandes, A. Cavaleiro, A.P. Tschiptschin, NbC-Ni coatings deposited by DC reactive magnetron sputtering: effect of Ni content on mechanical properties, thermal stability and oxidation resistance, Surf. Coat. Technol. 349 (2018) 1018–1031, https://doi.org/10.1016/j.surfcoat.2018.06.068.

[35] Y. Lv, L. Ji, X. Liu, H. Li, H. Zhou, J. Chen, The structure and properties of CrAlN films deposited by mid-frequency unbalanced magnetron sputtering at different substrate bias duty cycles, Surf. Coat. Technol. 206 (2012) 3961–3969, https://doi.org/10.1016/j.surfcoat.2012.03.068.

[36] T. Turutoğlu, M. Ürgen, A.F. Çakir, A. Öztürk, Characterization of Mo2N/Ag nanocomposite coatings produced by magnetron sputtering, Key Eng. Mater. 264–268 (2004) 489–492, https://doi.org/10.4028/www.scientific.net/kem.264-268.489.

[37] A. Vyas, Z.F. Zhou, Y.G. Shen, Effect of aluminum contents on sputter deposited CrAlN thin films, IOP Conf. Ser.: Mater. Sci. Eng. 307 (2018), https://doi.org/10.1088/1757-899X/307/1/012079.

[38] Z. Li, P. Munroe, Z.T. Jiang, X. Zhao, J. Xu, Z.F. Zhou, J.Q. Jiang, F. Fang, Z.H. Xie, Designing superhard, self-toughening CrAlN coatings through grain boundary engineering, Acta Mater. 60 (2012) 5735–5744, https://doi.org/10.1016/j.actamat.2012.06.049.

[39] A. Al-Rjoub, P. Costa, L. Rebouta, M.F. Cerqueira, P. Alpuim, N.P. Barradas, E. Alves, Characterization of magnetron sputtered sub-stoichiometric CrAlSiNx and CrAlSiOyNx coatings, Surf. Coat. Technol. 328 (2017) 134–141, https://doi.org/10.1016/j.surfcoat.2017.08.038.

[40] P. Kumari, P. Majewski, Adsorption of albumin on silica surfaces modified by silver and copper nanoparticles, J. Nanomater. 2013 (2013), https://doi.org/10.1155/2013/839016.

[41] J. Sharma, N.K. Chaki, A.B. Mandale, R. Pasricha, K. Vijayamohanan, Controlled interlinking of Au and Ag nanoclusters using 4-aminothiophenol as molecular interconnects, J. Colloid Interface Sci. 272 (2004) 145–152, https://doi.org/10.1016/j.jcis.2003.09.016.

[42] Z. Zhang, X. Zhang, Z. Xin, M. Deng, Y. Wen, Y. Song, Synthesis of monodisperse silver nanoparticles for ink-jet printed flexible electronics, Nanotechnology. 22 (2011), https://doi.org/10.1088/0957-4484/22/42/425601.

[43] M.H. Habibi, R. Sheibani, Nanostructure silver-doped zinc oxide films coating on glass prepared by sol-gel and photochemical deposition process: application for removal of mercaptan, J. Ind. Eng. Chem. 19 (2013) 161–165, https://doi.org/10.1016/j.jiec.2012.07.019.

[44] N.K. Manninen, R.E. Galindo, N. Benito, N.M. Figueiredo, A. Cavaleiro, C. Palacio, S. Carvalho, Ag-Ti(C, N)-based coatings for biomedical applications: influence of silver content on the structural properties, J. Phys. D. Appl. Phys. 44 (2011), https://doi.org/10.1088/0022-3727/44/37/375501.

[45] Z.B. Qi, Z.T. Wu, Z.C. Wang, Improved hardness and oxidation resistance for CrAlN hard coatingswith Y addition by magnetron co-sputtering, Surf. Coat. Technol. 259 (2014) 146–151, https://doi.org/10.1016/j.surfcoat.2014.02.034.

[46] Y.X. Wang, S. Zhang, J.W. Lee, W.S. Lew, B. Li, Influence of bias voltage on the hardness and toughness of CrAlN coatings via magnetron sputtering, Surf. Coat. Technol. 206 (2012) 5103–5107, https://doi.org/10.1016/j.surfcoat.2012.06.041.

[47] N. Bagcivan, K. Bobzin, S. Theiß, (Cr1 - XAlx)N: a comparison of direct current, middle frequency pulsed and high power pulsed magnetron sputtering for injection molding components, Thin Solid Films 528 (2013) 180–186, https://doi.org/10.1016/j.tsf.2012.08.056.

[48] B. Trindade, W.Z. Li, F. Fernandes, A. Cavaleiro, Effect of Nb target power on the structure, mechanical properties, thermal stability and oxidation resistance of Cr-Al-Nb-N coatings, Surf. Coat. Technol. 285 (2016) 270–277, https://doi.org/10.1016/j.surfcoat.2015.12.002.

[49] A.G. Bembel, On the size dependences of the metallic nanoparticle evaporation and sublimation heats: thermodynamics and atomistic modeling, Russ. Phys. J. 59 (2017) 1567–1574, https://doi.org/10.1007/s11182-017-0945-6.

[50] V.M. Samsonov, S.A. Vasilyev, A.G. Bembel, Size dependence of the melting temperature of metallic nanoclusters from the viewpoint of the thermodynamic theory of similarity, Phys. Met. Metallogr. 117 (2016) 749–755, https://doi.org/10.1134/S0031918X16080135.

[51] M.A. Asoro, D. Kovar, P.J. Ferreira, In situ transmission electron microscopy observations of sublimation in silver nanoparticles, ACS Nano 7 (2013) 7844–7852, https://doi.org/10.1021/nn402771j.

[52] A. Liu, J. Deng, H. Cui, J. Zhao, X. Ai, Oxidation resistance of CrN and CrAlN coating tools, Adv. Mater. Res. 189–193 (2011) 137–141, https://doi.org/10.4028/www.scientific.net/AMR.189-193.137.
[53] W. Garkas, S. Weiß, Q.M. Wang, (Cr1-xAlx)N as a candidate for corrosion protection in high temperature segments of CCS plants, Environ. Earth Sci. 70 (2013) 3761–3770, https://doi.org/10.1007/s12665-013-2646-y.
[54] T.P. Li, X.H. Yin, M.S. Li, Y.C. Zhou, Oxidation resistance of a Cr 0.50Al 0.50N coating prepared by magnetron sputtering on alloy K38G, Oxid. Met. 68 (2007) 193–210, https://doi.org/10.1007/s11085-007-9069-7.
[55] J. Lin, B. Mishra, J.J. Moore, W.D. Sproul, A study of the oxidation behavior of CrN and CrAlN thin films in air using DSC and TGA analyses, Surf. Coat. Technol. 202 (2008) 3272–3283, https://doi.org/10.1016/j.surfcoat.2007.11.037.
[56] S. Hofmann, H.A. Jehn, Oxidation behavior of CrNx and (Cr,Al)Nx hard coatings, Mater. Corros. 41 (1990) 756–760, https://doi.org/10.1002/maco.19900411222.
[57] Y.P. Wu, H.Y. Chiang, H.I. Hsiang, AgCrO2 formation mechanism during silver inner electrode and Fe–Si–Cr alloy powder co-firing in metal multilayer chip power inductors, J. Mater. Sci. Mater. Electron. 0 (2019) 0, https://doi.org/10.1007/s10854-019-01130-5.
[58] A.A.H. El-Bassuony, H.K. Abdelsalam, Tailoring the structural, magnetic and antimicrobial activity of AgCrO2 delafossite at high annealing temperature, J. Therm. Anal. Calorim. 138 (2019) 81–88, https://doi.org/10.1007/s10973-019-08207-7.
[59] A.v. Bondarev, D.G. Kvashnin, I.v. Shchetinin, D.v. Shtansky, Temperature-dependent structural transformation and friction behavior of nanocomposite VCN-(Ag) coatings, Mater. Des. 160 (2018) 964–973, https://doi.org/10.1016/j.matdes.2018.10.029.